Vol. 19, No. 2 (2020) 867-875
Revista Mexicana de Ingeniería Química

Swirling fluidized bed plasma reactor for the preparation of supported nanoparticles

Reactor de plasma de lecho fluidizado giratorio para la preparación de nanopartículas soportadas

G. Soto[1]*, E. Pahuamba[2], F. Ramirez[2], J. Cruz-Reyes[3], M. Del Valle[3], H. Tiznado[1]

[1] *Universidad Nacional Autónoma de México, Centro de Nanociencias y Nanotecnología, Km. 107 Carretera Tijuana-Ensenada, México.*

[2] *Centro de Investigación Científica y Educación Superior de Ensenada. Posgrado en Física de Materiales, Km. 107 Carretera Tijuana-Ensenada, México.*

[3] *Universidad Autónoma de Baja California, Facultad de Ciencias Químicas e Ingeniería, Calzada Tecnológico 14418 Mesa de Otay, Tijuana, México.*

Received: September 24, 2019; Accepted: October 31, 2019

Abstract

A swirling fluidized bed reactor design for the preparation of supported nanoparticles is reported. It uses a DC plasma torch that decomposes and vaporizes salt precursors; the cationic part condenses as metal nanoparticles on a powder support. Any fluidizable granular material can be used as support, as long as it withstands the temperatures of the plasma torch. The torch is located at the center of the reactor axis and the powder is fluidized using a cyclonic action (swirl) to minimize the space where the grains could come into direct contact with the plasma zone. The reactor was tested for silver nanoparticles (AgNPs) supported on silica-alumina, using silver nitrate as precursor. The results show large grains decorated with nano-sized metal particles. Depending on the load of silver nitrate, the size of the nanoparticles can range from 3 to 50 nm, as measured using transmission electron microscopy. They are in a non-oxidized state, as revealed with x-ray photoelectron spectroscopy. The AgNPs/SiO_2-Al_2O_3 composite was tested as a catalyst in the hydrodesulphurization of dibenzothiophene. This method can be scaled up to produce large quantities of supported metallic particles. Its inherent simplicity, high processing speed and the low operating cost are its main advantages.

Keywords: silver nanoparticles, fluidized bed, swirling bed, plasma reactor, hydrodesulphurization.

Resumen

Se presenta un reactor de lecho fluidizado con acción ciclónica para preparar nanopartículas soportadas. Se usa una antorcha de plasma DC que descompone y vaporiza precursores salinos. La parte catiónica condesa como partículas metálicas en el soporte. Cualquier polvo fluidizable puede ser usado como soporte en tanto resista las temperaturas del reactor. La antorcha está situada en el eje central del reactor y los polvos son fluidizados usando acción ciclónica para minimizar el espacio donde los granos podrían entrar en contacto con el plasma. El reactor fue probado para producir nanopartículas de plata (AgNPs) que fueron soportadas en sílice-alúmina a partir de nitrato de plata. Los resultados muestran granos decorados con partículas metálicas de tamaño nanométrico. Dependiendo de la carga de precursor, el tamaño de las AgNPs puede ir de 3 a 50 nm, como fue medido por microscopia electrónica de transmisión y además se encuentran en estado no-oxidado, según fue determinado por XPS. El compósito resultante, AgNPs/SiO_2-Al_2O_3, se probó como catalizador en la reacción de hidrodesulfuración de dibenzotiofeno. El reactor presentado puede ser escalado para producir grandes cantidades de partículas soportadas. Su simplicidad, su alta velocidad y el bajo costo operativo son sus principales ventajas.

Palabras clave: nanopartículas de plata, lecho fluidizado, acción ciclónica, reactor de plasma, hidrodesulfuración.

* *Corresponding author. E-mail*: gerardo@cnyn.unam.mx

https://doi.org/10.24275/rmiq/Mat886
issn-e: 2395-8472

1 Introduction

Nanotechnology works at or near the atomic level to create new materials with beneficial physical properties and behaviors. The development of diverse products that can solve long-standing problems and facilitate unprecedented applications depends on the conception of large-scale and low-cost manufacturing process of nanomaterials (Petronella *et al*., 2019) (Su & Chang, 2017). Although new methods for the synthesis of nanomaterials are conceived every week, only some of them are suitable to be scaled for mass production at a reasonably low cost (Brabazon *et al*., 2017). Previously we reported a fluidized-bed microwave plasma reactor for the production of supported metallic particles (Soto *et al*., 2011). In that article the synthesis of Silver Nanoparticles (AgNPs) over silica powder was used to establish the capabilities of our design. The resulting material exhibited good catalytic and antibacterial properties. While the goal of scalable configuration for mass-production was attained in that work, that design had some drawbacks. For instance, the use of microwave plasma requires the use of vacuum to create the conditions for plasma ignition at low-power levels, or else, a very high power magnetron is required when the reactor is to be operated at atmospheric pressures. Both of these solutions are somewhat expensive for large-scale production. To address these limitations a new plasma reactor design is proposed in this work, which operates at atmospheric pressure by the use of Direct Current (DC) plasma. For that purpose, we used a commercially available DC-cutter torch as the plasma source. At first glance this is a straightforward move; however, there are some technical difficulties that needed to be resolved in order to make a fully functional design. The main concern is the plasma distribution within the reactor; that is, while the microwave plasma is distributed almost homogeneously within the reactor volume, in DC the plasma is concentrated in the nozzle of the torch. Thereafter, the power density increases several orders of magnitude in the close proximity to the torch. Under these circumstances hot-spots are created inside the reactor that can easily melt the powders. Typical temperatures obtained in a plasma jet torch may be of the order of 10,000 K (Wang *et al*., 2010), so the torch has the ability to melt and sinter any material that comes into direct contact with it. Therefore, a solution must be designed to prevent the grains from clumping during the operation of the reactor. A relatively new variant in fluidized bed technology called Swirling Fluidized Bed (SFB) – where the grains describe a helical path adjacent to the walls of the container – is very convenient for our purposes. The key difference of SFB is the incorporation of momentum in both, the radial and tangential directions (Chyang & Yen-Chin, 2002), leaving a diluted central portion of the ascending column which is surrounded by a dense layer of solids close to the wall of container (Sobrino *et al*., 2009). Several papers have been published studying the flow dynamics of SFB (Naz *et al*., 2019; Sirisomboon & Laowthong, 2019; Tawfik *et al*., 2019) and it is expected that this technological innovation will find applications in different fields of technology (Yudin *et al*., 2016).

The aim of this work is to show the SFB reactor design using a DC plasma torch and to prove that the resulting materials are equivalent to those produced by the microwave reactor (Soto *et al*., 2011). With that aim, we have produced silver nanoparticles over silica-alumina support and characterized them with several analytical techniques, like electron microscopy, x-ray photoelectron spectroscopy, infrared and CO absorption (supplementary data). We conclude that the resulting materials are equivalent to those produced by microwave plasma and low pressures.

2 Experimental

2.1 Reactor design

The reactor is based on an upward flow capable of fluidizing fine powder grains, but keeping the powder particles out of the central axis of the reactor, where the plasma source is placed. Fig. 1 is a scheme of the Plasma Swirling Fluidized Bed Reactor (P-SFB). The body of the reactor is a quartz tube, 22 mm internal diameter and 0.5 m long. The fumes exhaust is at the top, the plasma torch and gas inputs are at the bottom. The crucial piece of this setup is the vortex generator, which is shown in the bottom of Fig. 2. It follows the concept of reference (Hansen, 2014), but with some modifications. The vortex generator consists of a cone situated at the base of a quartz tube with three tangential slanted nozzle-jet orifices. Each orifice is at 120° of each other. The reactor was designed around a commercially available 3.5 kW DC-cutter torch as plasma source (Multiplaz model 3500, Switzerland) in order to provide plasma energy for salt decomposition

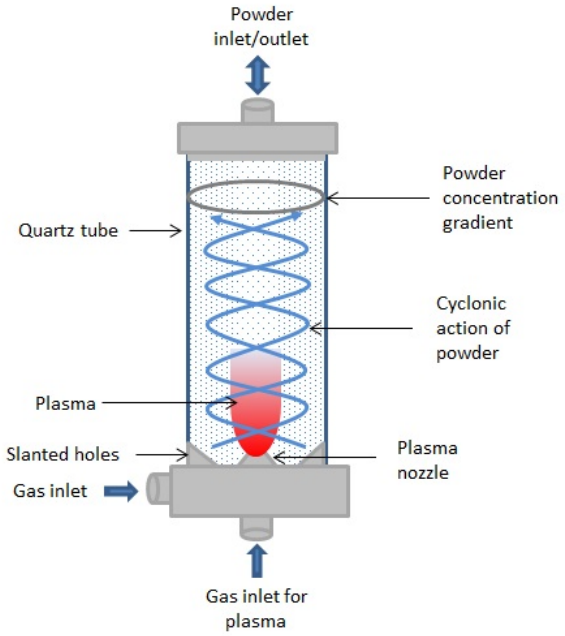

Fig 1. Outline of the fluidized bed reactor with swirl action. The flow distributor is a cone with three jet holes at 120 ° between them; the orifices have been inclined with a tangential component to produce an helicoidal flow inside the tube.

Fig 2. Photographs of the Plasma SFB in operation (top) and the flow distributor cone with slanted jet orifices and a central hole for the plasma torch (see video in supplementary data).

and vaporization.

2.2 *Material synthesis*

For this application, a 90 % silica-10 % alumina powder is used as the substrate. The powder is specified as grade 135, and mesh -100, available from Aldrich as a catalyst support. For the experiments presented here the silica alumina powder is dried off in a beaker at approximately 423 K. Once the powder is at room temperature, it is mixed with silver nitrate ($AgNO_3$, 99.95 %) at the weight ratios listed in Table 1. Next the powder is thoroughly ground in an agate mortar until the mixture becomes homogeneous in color and grain size. Then, the mixture is placed into the bottom of the reactor. Before igniting the plasma, a N2 flow is admitted by way of the vortex generator to lift the powder bed. To ignite the plasma, a nitrogen influent is admitted via the plasma torch, see video 2 of supplementary data. The steady state plasma parameters are 200 V, 3 A, electrode distance 1 mm. The plasma is sustained 2 min; after that the reactor is cooled down and the powder is recovered from the reactor. There is an evident color change from white to pale brown as a function of the silver nitrate load.

2.3 *Material characterizations*

After the powders are processed in the SFB reactor, the resulting materials are extracted from the quartz tube and analyzed using several techniques. The morphology and particle dispersion were evaluated under electron microscopy. A scanning electron microscope, Jeol JSM-5300, with an auxiliary Energy Dispersive X-ray microanalysis (EDX), Noran Superdry II, was used to provide an overview of the morphology and chemical composition of the resulting powder. The processed materials were attached to a double-sided conductive carbon tape to perform the SEM analyzes. Composition was also evaluated using Inductively Coupled Plasma Optical Emission Spectrometry (ICP-OES) Varian, Vista-MPX. Transmission Electron Micrographs (TEM) were acquired using a Jeol JEM2010 instrument operated at 200 KeV. The samples for TEM were prepared by ultrasonically dispersing the powders in isopropyl alcohol and dropping the solution in a 300 mesh sample-grid. To determine the chemical oxidation state of the silver particles, an X-ray Photoelectron Spectroscopy (XPS) apparatus with a MAC-3 energy analyzer from CAMECA was employed.

Table 1 Proportion between support and reactive precursor.

Sample Label	Precursor /mg ($AgNO_3$)	Support / mg (SiO_2-Al_2O_3)	Expected Ag/Si ratio (atomic)	Ag / Si **ICP**	Ag /Si **EDS**
Ag0	0	5 000	-	< 0.0001	undetected
Ag1	25	5 000	0.002	0.001	undetected
Ag2	50	5 000	0.003	0.004	0.010
Ag3	100	5 000	0.007	0.012	0.011
Ag4	200	5 000	0.014	0.016	0.020
Ag5	500	5 000	0.035	0.020	0.026

The XPS data were collected using a non-monochromatic Al Kα X-ray line (1486.6 eV). The energy scale was calibrated using the reference binding energy of Cu $2p_{3/2}$ at 932.67 eV and Ag $3d_{5/2}$ at 368.26 eV, with an energy resolution of 1.1 eV. The charging effect was compensated by using the Si 2p line from the silica substrate, at 103.2 eV, as reference.

2.4 Catalytic activity measurements

The catalytic activity test was performed for the hydrodesulphurization (HDS) of dibenzothiophene (DBT) in a high pressure 300 mL Parr reactor. The by-products were sampled with an Agilent 6890 gas chromatograph using a 30 m HP-5 capillary column and a Flame Ionization Detector. Samples were taken every 20 min during the first hour, then every 30 min for the next 4 h. Reduction of sample volume due to sampling was ≤ 5% of total volume. Catalytic activity was expressed in terms of % conversion of DBT vs reaction time, and from this data the reaction rate constant, k', was calculated for each catalyst using the integrated formula of the zero order rate law: $X = k't$, where X is the DBT conversion fraction and t is the reaction time in minutes. A plot of X *vs* time, by linear regression, gives k' as the slope of the plot. The specific rate constant, k, for the catalyst is then calculated by:

$$k = k'(n_{DBT})\left(\frac{1}{60}\right)\left(\frac{1}{W_{cat}}\right) = [\text{mol / g·s}] \qquad (1)$$

where n_{DBT} is the initial amount of DBT in moles and W_{cat} is the weight of the recovered catalyst in grams. The mean standard deviation for catalytic measurements is estimated in 2.5%.

3 Results and discussion

The inclined flow of gas through the cone distributor produces two velocity components: the vertical component causes fluidization, while the horizontal components causes the swirling motion in bed (Yudin *et al*., 2016). As seen in video 1 in supplementary data (Soto, 2019), the high speed flow of these orifices generate a swirl with enough force to lift the powder bed. Without the gas supply the powder bed is in the lower part of the cone. As the gas is admitted a helical flow is induced, and consequently the powder bed starts to spin and lift up to the desired height as a function of admission pressure. As seen in video 1 and due to the centrifugal acceleration, the solid particles remain adjacent to the walls of the quartz tube, producing an exhausted portion in the center of the ascending column. Unlike a normal FB, where the particles rise and then fall because of the ascending hydrodynamic force and gravity (Mortier *et al*., 2011), in our SFB the particles remain at a nearly constant height due to the friction force between the particles and the walls of the container. This configuration does not require a distributor grid for fluidization, so it is very suitable for our application since the DC plasma torch can be located at the center axis of the reaction chamber, as illustrated in Fig. 2 where it is at the bottom of cone. Due to the high power density of the plasma, the inlet pressure was regulated to maintain the bed close to the upper portion of the plasma jet; see video 2 of supplementary data (Soto, 2019). In the experiments carried without the swirling effect the powder was almost completely sintered, which is undesirable for our purposes. It happens that a relatively small portion of the powder sinters even using swirling and precipitates in the form of granules.

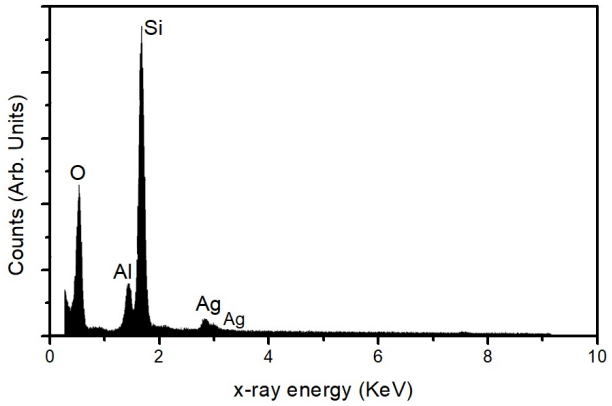

Fig 3. EDS spectrum of a silica-alumina powder processed with $AgNO_3$ as the precursor of AgNPs (Ag4 sample).

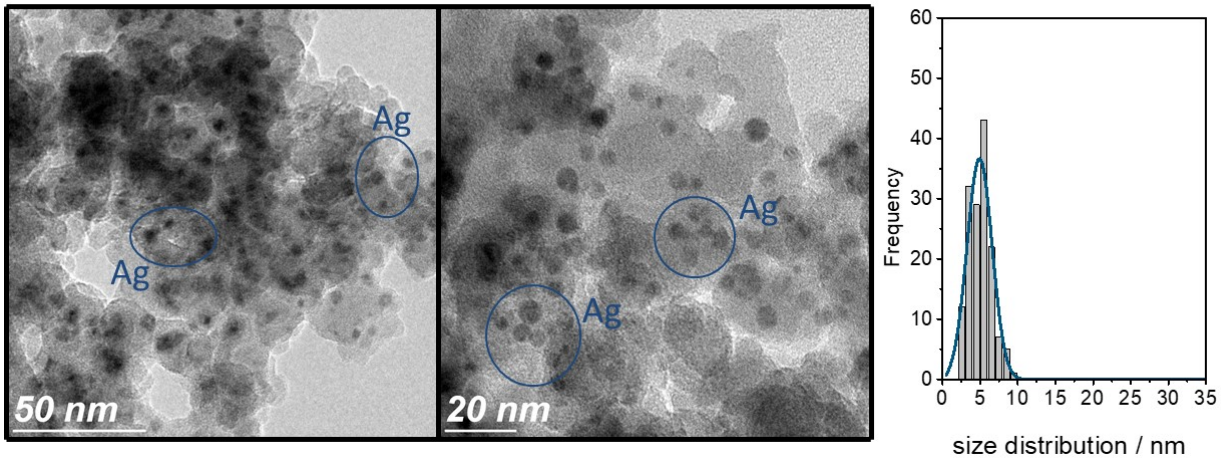

Fig 4. TEM micrograph and the unimodal particle distribution histogram for the Ag1 Sample. The decoration of the silica-alumina support with AgNPs is uniform.

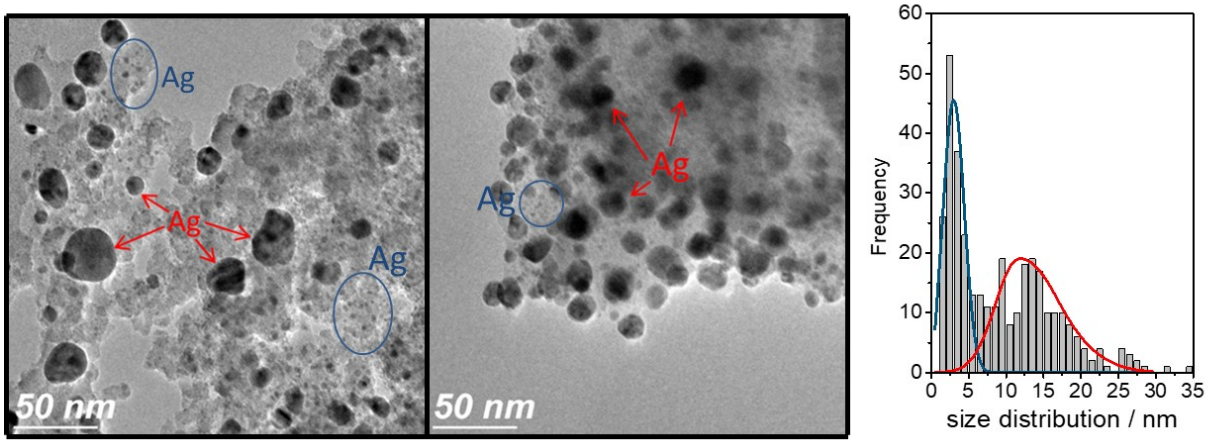

Fig 5. AgNPs dispersed in the silica-alumina granules for Ag4 Sample. Blue circles signpost small particles; red arrows for larger particles. The histogram shows a bimodal distribution of sizes.

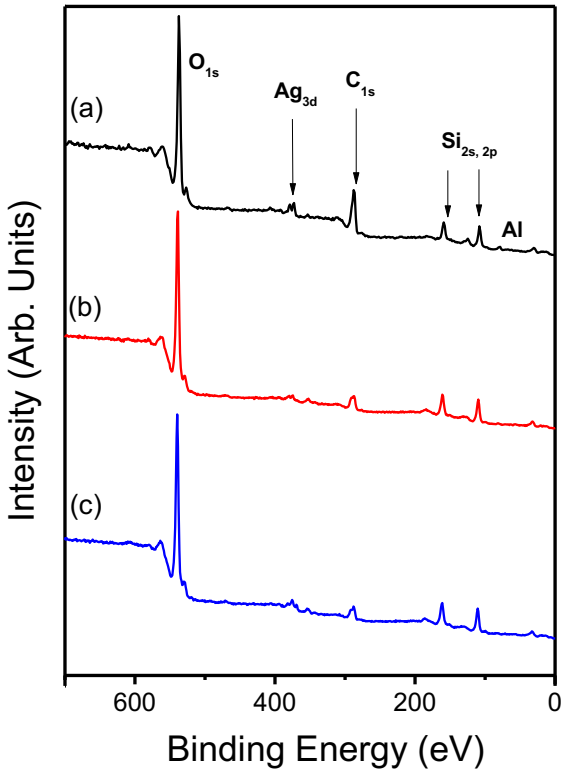

Fig 6.- Low resolution XP spectra for three samples: Ag5 in (a); Ag3 in (b) and Ag1 in (c).

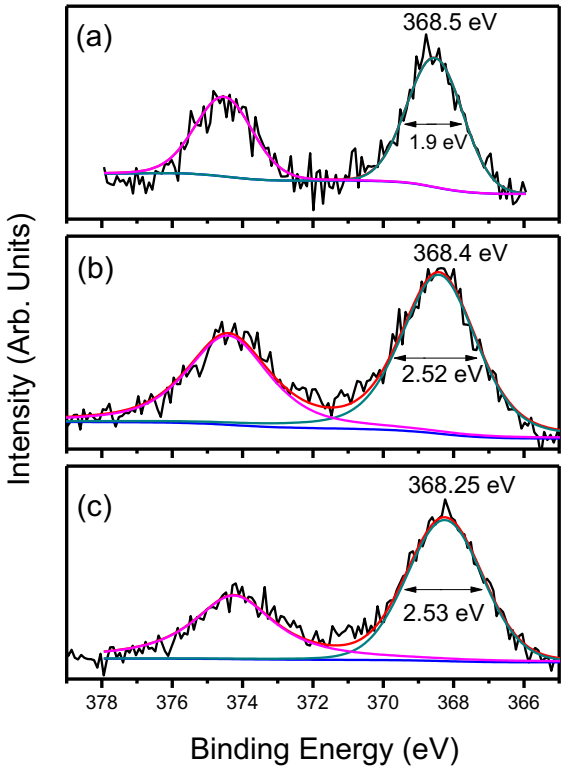

Fig 7.- High resolution XP spectra for (a) Ag1; (b) Ag3 and (c) Ag5 samples. The peak width increases as a function of the silver loading. The Ag_{3d} edge at 368.5 eV indicates the metallic character of the silver nano-clusters.

Table 1 shows the preparation conditions together with the expected and determined compositions by means of EDS and ICP-OES. While the measured atomic concentration increases with the silver nitrate load, there is an overestimation for low concentrations and an underestimation for high concentrations. Given that part of the silver forms a thin film on the walls of the container, the measured concentrations deviate from those expected. Fig. 3 shows an illustrative EDS spectrum; this for the Ag4 sample. Only the peaks corresponding to Si, Al, O and Ag are noticeable. There are not traces of elements related to the reactors components, as is Cu that could shed from the plasma jet nozzle; neither is there Fe from the stainless steel vortex generator. The same observations were made in all samples and corroborated by means of ICP-OES.

A collection of TEM images, Figs. 4-5, illustrates the representative characteristics of the AgNPs which were grown with the Plasma SFB reactor. Fig. 4 correspond to the AgNps produced at low $AgNO_3$ loads (Ag1 sample), while Fig. 5 is for high $AgNO_3$ loads (Ag4 sample). When the silver content is low the nanoparticles are smaller and their size distribution is centered around a single narrow peak: 3-6 nm for Ag1 sample, as shown in the Fig. 4. In contrast, for high silver content a highly dispersed distribution of nanoparticles is found; such a distribution requires the superposition of two Gaussian functions, in this case one centered at 3 nm and the other around 14 nm. The complete distribution is the combination of a less dispersed population with smaller particle sizes, and a relatively large, highly dispersed one with much larger particle sizes. All the observed particles displayed a crystalline nature, and some of the particles exhibited facets as well. Even the smaller Ag particles, which were 3 to 5 nm in diameter, present a crystalline nature. It is therefore clear that the reactor produces nanoparticles, and the size thereof, depends on the initial loading of silver precursor.

The general chemical composition of processed powders and the chemical oxidation of silver were studied by means of XPS. Fig. 6 is low resolution XPS scan. The main transitions originate from the substrate (Si, Al and O) with adventitious C, which most probably results from ambient contamination.

Table 2. Activity and selectivity results in the HDS of DBT of the different AgNPs catalysts prepared by plasma swirling fluidized bed.

Sample	CHCPM %	DCH %	PCH %	BP %	THDBT %	DBT %	HYD/DDS	$k(\times 10^{-7})$ mol/g·s
Ag0	0	0	0.40	3.33	0.866	95.4	0.378	5.6
Ag1	0.269	0	1.04	4.13	1.70	92.85	0.664	12.98
Ag2	0	0	0.654	3.87	1.26	94.21	0.494	10.93
Ag3	0.30	0	1.25	4.32	2.22	91.89	0.805	22.23
Ag5	0.366	0	1.465	4.55	2.61	90.99	0.89	26.2

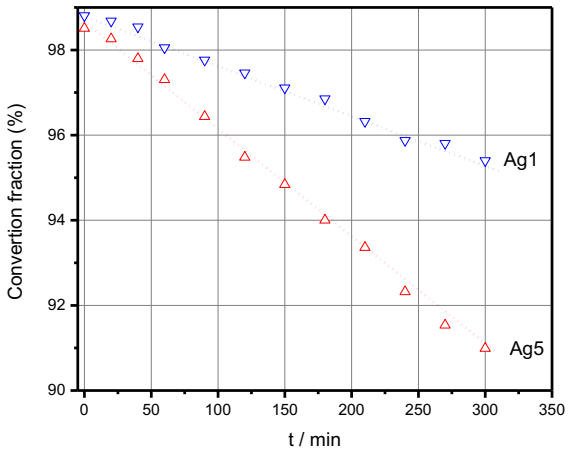

Fig 8- Plot of conversion rate vs. reaction time for the HDS of DBT.

No further elements were detected. Fig. 7 shows high resolution spectra around the Ag-3d energy window for representative samples: Ag1, Ag3 and Ag5. The charge shifting was corrected using the energy for Si 2p on SiO_2 at 103.3 eV. The energy value for the Ag 3d peak at 368.3 eV indicates that silver is present in a non-oxidized state: Ag^0. The widening of peaks increases with the silver nitrate loading, indicative of a greater dispersion of chemical states in samples with high silver content. This is further studied in the supplementary data by means of FTIR-CO absorption(Soto *et al*., 2019).

The catalytic activity in the HDS conversion of DBT for Ag1 and Ag5 samples are plotted in Fig. 8. The linear behavior in the reaction mixture, X, vs reaction time, t, reveal a zero order rate law. The rate constants of these samples are greater than the rates of nanostructured molybdenum sulfides (3.5×10^{-7} mol/g·s) reported (Camacho-Bragado *et al*., 2005). The ratio between the most active catalyst (Ag5 sample) and the reference; that is, the processed support without silver nitrate (Ag0 sample) is around 4.67, highlighting the influence of the AgNPs on the catalytic activity. The k values for the samples increase with the amount of silver, from 12.9 to 26.2×10^{-7} mol/g·s. Table 2 summarizes the activity and selectivity in the HDS of DBT for the different samples. The HDS of DBT might follows two parallel pathways, yielding mainly biphenyl (BP) through the direct desulfurization (DDS) pathway; and phenylcyclohexane (PCH) and tetrahydrodibenzothiophene (THDBT) through the hydrogenation (HYD) pathway. Other HYD derived products are cyclohexylcyclopentylmethane (CHCPM) and dicyclohexyl (DCH). The selectivity is generally accepted by the HYD/DDS ratio (Isoda *et al*., 1996), see Table 2. The HYD/DDS ratio, is calculated by the following equation (Isoda *et al*., 1996):

$$\frac{HYD}{DDS} = \frac{[CHB] + [THDBT]}{[BP]} \tag{2}$$

All the samples favored the direct desulfurization path, detecting BP as the main byproduct.

Conclusions

We have presented sufficient evidence of the preparation of supported nanoparticles from solid state precursors using a new approach. In this case the Plasma SFB reactor was tested using AgNPs over a silica-alumina support, but many different reactants could be used as well. The most prominent particle size was approximately 5 nm in diameter, and the largest are always below 50 nm, however these are rarely encountered. The catalyst function, as shown here, requires that many atoms be available to assist the desired reaction; therefore, smaller nanoparticles make the best catalysts because they are well dispersed with many active sites. As the properties of this composite agree with the physical characteristics expected for this material we can conclude that the synthesis has been successful. The plasma is the driving force for the decomposition of precursors,

which induces its atomization and the subsequent condensation in the form of nanoparticles on the surface of the silica granules, which act as supports. However, the plasma distribution within the reactor is concentrated in the nozzle of the torch. As the power density is very high, it can easily melt the powders that come into contact with the plasma zone. The swirl behavior of the FB limits the distribution of particles near the wall of the container, creating a depleted space along the axis of the reactor. In this way, the contact between plasma and swirling particles is minimized.

The technique offers an easy method to grow stable nanoparticles, as demonstrated. The performance of the AgNPs/silica-alumina composite for the HDS reaction, which is similar to that of MoS_2 based catalysts, was exemplified. Compared to related methods that produce supported nanoparticles, the inherent simplicity of the Plasma SFB method is its main advantage, and for this reason it could be easily scaled-up for industrial production. As far as we know, this is the first implementation of a SFB for the preparation of nanomaterials.

Acknowledgements

The authors would like to thank L. López Sosa, I. Velázquez Hernández, Francisco Ruiz, Jaime Mendoza, Jesús A. Díaz, Israel Gradilla, E. Murillo, P. Piza, and Eloisa Aparicio for their technical assistance. The use granted by the UABC laboratories for gas chromatography analysis is highly appreciated.

Funding information

This work was supported by UNAM-DGAPA-PAPIME PE100318, PE101317 and UNAM-DGAPA-PAPIIT IA 101018, IN 112117, IN 110018, and IA 103117 projects as well as by Conacyt through Fordecyt 272894 project.

References

Brabazon, D., Pellicer, E., Zivic, F., Sort, J., Baró, M. D., Grujovic, N., & Choy, K. L. (2017). Commercialization of nanotechnologies-A case study approach. *Commercialization of Nanotechnologies-A Case Study Approach*. Springer International Publishing. https://doi.org/10.1007/978-3-319-56979-6

Camacho-Bragado, G. A., Elechiguerra, J. L., Olivas, A., Fuentes, S., Galvan, D., & Yacaman, M. J. (2005). Structure and catalytic properties of nanostructured molybdenum sulfides. *Journal of Catalysis 234*, 182-190. https://doi.org/10.1016/j.jcat.2005.06.009

Chyang, C.-S., & Yen-Chin, L. (2002). A study in the swirling fluidizing pattern. *Journal of Chemical Engineering of Japan 35*, 503-512. https://doi.org/10.1252/jcej.35.503

Hansen. (2014). (12) United States Patent S371 (c)(1), (2), (4) Date. Retrieved from https://patentimages.storage.googleapis.com/85/03/c0/b73a966debb322/US8110155.pdf

Isoda, T., Nagao, S., Ma, X., Korai, Y., & Mochida, I. (1996). Hydrodesulfurization of refractory sulfur species. 1. Selective hydrodesulfurization of 4,6-dimethyldibenzo-thiophene in the major presence of naphthalene over $CoMo/Al_2O_3$ and Ru/Al_2O_3 blend catalysts. *Energy & Fuels 10*, 482-486. https://doi.org/10.1021/ef950144c

Mortier, S. T. F. C., De Beer, T., Gernaey, K. V, Remon, J. P., Vervaet, C., & Nopens, I. (2011). Mechanistic modelling of fluidized bed drying processes of wet porous granules: a review. *European Journal of Pharmaceutics and Biopharmaceutics?: Official Journal of Arbeitsgemeinschaft Für Pharmazeutische Verfahrenstechnik e.V, 79*, 205-225. https://doi.org/10.1016/j.ejpb.2011.05.013

Naz, M. Y., Shukrullah, S., Sulaiman, S. A., Khan, Y., Alkanhal, M. A. S., & Ghaffar, A. (2019). Particle image velocimetry analysis of a swirling bed operation by using a mesh-coupled annular air distributor. *Journal of the Brazilian Society of Mechanical Sciences and Engineering 41*. https://doi.org/10.1007/s40430-019-1857-x

Petronella, F., Truppi, A., Dell?Edera, M., Agostiano, A., Curri, M. L., & Comparelli, R. (2019, June 1). Scalable synthesis of mesoporous TiO_2 for environmental photocatalytic applications. *Materials*. MDPI AG. https://doi.org/10.3390/ma12111853

Sirisomboon, K., & Laowthong, P. (2019). Experimental investigation and prediction

of heat transfer in a swirling fluidized-bed combustor. *Applied Thermal Engineering*, 718-727. https://doi.org/10.1016/j.applthermaleng.2018.10.097

Sobrino, C., Ellis, N., & de Vega, M. (2009). Distributor effects near the bottom region of turbulent fluidized beds. *Powder Technology 189*, 25-33. https://doi.org/10.1016/J.POWTEC.2008.05.012

Soto, Gerardo; Tiznado, Hugo; Pahuamba, E. (2019). FTIR spectra of CO adsorbed on silica-alumina supported silver nanoparticles. *Mendeley Data 2*. https://doi.org/10.17632/YJCSKHF6HM.2

Soto, G. (2019). Mendeley Data. https://doi.org/http://dx.doi.org/10.17632/zf9mjpxkvy.1

Soto, G., Tiznado, H., Contreras, O., Pérez-Tijerina, E., Cruz-Reyes, J., Del Valle, M., & Portillo, A. (2011). Preparation of a Ag/SiO_2 nanocomposite using a fluidized bed microwave plasma reactor, and its hydrodesulphurization and Escherichia coli bactericidal activities. *Powder Technology 213*, 55-62. https://doi.org/10.1016/j.powtec.2011.07.005

Su, S. S., & Chang, I. (2017). Review of production routes of nanomaterials. In *Commercialization of Nanotechnologies-A Case Study Approach* (pp. 15-29). Springer International Publishing. https://doi.org/10.1007/978-3-319-56979-6_2

Tawfik, M. H. M., Refaat Diab, M., & Mohmed Abdelmotalib, H. (2019). An experimental investigation of wall-bed heat transfer and flow characteristics in a swirling fluidized bed reactor. *Applied Thermal Engineering*, 501-507. https://doi.org/10.1016/j.applthermaleng.2019.04.022

Wang, P.-J., Tzeng, C.-C., & Liu, Y. (2010). Thermal Temperature Measurements of Plasma Torch by Alexandrite Effect Spectropyrometer. *Advances in Optical Technologies 2010*, 1-7. https://doi.org/10.1155/2010/656421

Yudin, A. S. M., Anuar, S., & Oumer, A. N. (2016). Improvement on particulate mixing through inclined slotted swirling distributor in a fluidized bed: An experimental study. *Advanced Powder Technology 27*, 2102-2111. https://doi.org/10.1016/J.APT.2016.07.023